Strength, stiffness and ductility of concrete-filled steel columns under axial compression

Zhi-Bin Wang [a,b], Zhong Tao [b,*], Lin-Hai Han [c], Brian Uy [d], Dennis Lam [e], Won-Hee Kang [b]

[a] *College of Civil Engineering, Fuzhou University, Fuzhou, Fujian Province 350108, China*

[b] *Centre for Infrastructure Engineering, Western Sydney University, Penrith, NSW 2751, Australia*

[c] *Department of Civil Engineering, Tsinghua University, Beijing 100084, China*

[d] *School of Civil Engineering, The University of Sydney, Sydney, NSW 2006, Australia*

[e] *School of Engineering, University of Bradford, Richmond Road, Bradford BD7 1DP, United Kingdom*

ABSTRACT

Extensive experimental and theoretical studies have been conducted on the compressive strength of concrete-filled steel tubular (CFST) columns, but little attention has been paid to their compressive stiffness and deformation capacity. Despite this, strength prediction approaches in existing design codes still have various limitations. A finite element model, which was previously proposed by the authors and verified using a large amount of experimental data, is used in this paper to generate simulation data covering a wide range of parameters for circular and rectangular CFST stub columns under axial compression. Regression analysis is conducted to propose simplified models to predict the compressive strength, the compressive stiffness, and the compressive strain corresponding to the compressive strength (ductility) for the composite columns. Based on the new strength prediction model, the capacity reduction factors for the steel and concrete materials are recalibrated to achieve a target reliability index of 3.04 when considering resistance effect only.

Keywords: Concrete-filled steel tubes; Axial compression; Finite element analysis; Compressive strength; Compressive stiffness; Ductility.

* Correspondence author.
E-mail address: z.tao@westernsydney.edu.au (Z. Tao).

Nomenclature

A_c	Cross-sectional area of concrete
A_s	Cross-sectional area of the steel tube
B	Width of a rectangular cross-section
D	Diameter of a circular cross-section
D'	Equivalent diameter of a rectangular cross-section
EA	Compressive stiffness of a CFST stub column
E_c	Elastic modulus of concrete
E_s	Elastic modulus of steel
f_c'	Cylinder compressive strength of concrete
f_{cu}	Cube compressive strength of concrete
f_y	Yield stress of steel
f_u	Ultimate strength of steel
H	Cross-sectional height of a rectangular tube
L	Length of a CFST stub column
N_a	Strength contribution of the steel tube
N_c	Strength contribution of the concrete core
N_u	Ultimate strength of a CFST stub column
R^2	Coefficient of determination
SD	Standard deviation
t	Wall thickness of the steel tube
β	Reliability index for resistance
ε	Strain
ε_c	Compressive strain corresponding to the compressive strength
ϕ	Capacity reduction factor for steel
ϕ_c	Capacity reduction factor for concrete
κ_c	Correction factor for the concrete stiffness
μ	Average value
σ	Stress

1. Introduction

Concrete-filled steel tubular (CFST) members have been widely used in routine structural design as piles, building columns and bridge piers. This is due to the great advantages of composite members, including high strength, good ductility, high energy absorption capacity, and rapid construction. From the 1960s, behaviour of CFST members has been extensively investigated [1-4]. Accordingly, many design codes have been developed, such as the Japanese code AIJ [5], Australian code AS 5100 [6], European code EN1994 [7], American codes AISC [8] and ACI [9], and Chinese code DBJ 13-51-2010 [10]. For design purposes, all these codes have provided some limitations on material strengths and section slenderness, as summarised in Table 1. Beyond those limitations, the existing codes might give less accurate strength predictions [11,12]. Even within the limitations, the strength predictions from the existing codes show considerable deviation from the experimental results and the predication accuracy could be further improved [13-15].

In recent years, developments of high strength steel and concrete have progressed in leaps and bounds, and high strength CFST columns have already been used in some building structures. For example, the Latitude Building in Sydney used a steel grade of 690 MPa and 80 MPa strength concrete in box-shaped CFST sections in the two-storey, 7 m deep transfer trusses [16]. In Japan, the Obayashi Technical Research Institute Main Building used CFST columns with a steel grade of 780 MPa and concrete compressive strength of 160 MPa [17]. These applications highlight the urgent need to develop design methods to cope with the development of high-strength materials.

In investigating CFST stub columns under compression, previous studies have mainly focused on their compressive strength. Very little attention has been paid to their compressive stiffness and deformation capacity [18,19]. For structural analysis, compressive stiffness of a member affects the internal force distribution; therefore accurate values should be provided. Meanwhile, designers

nowadays are paying more attention to extreme loading, such as seismicity, impact and fire; and other abnormal events. Accordingly, the issue of ductility or deformation capacity is of considerable interests to the designers. The compressive strain corresponding to the ultimate strength to some extent reflects ductility or deformation capacity of an axially loaded CFST column, and simplified equations should be proposed to assist the designers.

A finite element (FE) model was previously developed by Tao et al. [20] for simulating circular and rectangular CFST stub columns under axial compression, which has been verified by a large amount of full-range load–deformation curves. The FE model will be used in this paper to generate simulation data to cover a wide range of parameters, and regression analysis will be conducted to propose simplified models to predict the compressive strength and corresponding strain, and compressive stiffness for the composite columns. Based on the new strength prediction model, the capacity reduction factors for the steel and concrete materials will be recalibrated.

2. Compressive strength predictions based on existing design codes

A database containing test results of 484 circular CFST stub columns and 445 rectangular CFST stub columns was used by Tao et al. [13] to evaluate the applicability of existing design codes, including AIJ, AISC, DBJ 13-51-2003 and EN1994, in calculating the compressive strength. It should be pointed out that the formulae presented in AS 5100: Part 6 are virtually the same as those suggested in EN1994 for compressive strength prediction. Therefore, the predicted results using AS 5100 are similar to those from EN1994. The evaluation conducted by Tao et al. [13] indicates that EN1994 has provided comparable predictions as DBJ 13-51-2003 for rectangular CFST stub columns, but gives better predictions than do the AIJ and AISC. In contrast, EN1994 gives better strength predictions than other design codes for circular CFST stub columns.

Although reasonable strength predictions are given by EN1994, considerable deviation from the experimental results was still reported by Tao et al. [13], Kuranovas et al. [14], and Güneyisi et al. [15]. This is also the case for other design codes. The deviations are mainly caused by unavoidable experimental errors, different specimen end conditions and variations in specimen preparation and quality. The influence of these factors is difficult, if not impossible, to be eliminated in code comparison. Another contributing factor to the variation is the limitations of the design codes themselves. For example, EN1994 considers the local buckling effect for circular thin-walled tubes by limiting the diameter (D) to thickness (t) ratio to $90\times235/f_y$ and the cross-sectional height (H) to thickness ratio (t) to $52\sqrt{235/f_y}$ for rectangular thin-walled tubes, where f_y is the yield stress of the steel tube. However, no details were given in the EN1994 on how to account for the local buckling effect if these limits were exceeded. Therefore, previous code comparisons simply ignored this specification to check the possibility of relaxing the section slenderness limitation.

The ambiguity in the definition of ultimate strength (N_u) is also a factor causing the deviation of prediction accuracy. This particularly becomes an issue for specimens without descending branches in their load–deformation curves. For most CFST columns demonstrating softening post-peak response, N_u is normally taken as the peak load corresponding to an axial strain of less than 0.01. But CFST columns with compact sections, high-strength steel or low-strength concrete may not have a softening response or may demonstrate softening at a very late stage. In this case, ultimate strength was often arbitrarily determined by researchers. The majority of researchers simply reported the maximum loads obtained at a very large axial strain, most likely at the end of testing. Those maximum loads were later used in the database for code comparison. An example is shown in Fig. 1, where the circular CFST specimen C7 with compact section was tested by Giakoumelis and Lam [21]. This specimen had a diameter-to-thickness ratio (D/t) of 23.4 and a length (L) of

300.5 mm. The yield stress of steel (f_y) and compressive cube strength of concrete (f_{cu}) were 365 and 34.7 MPa, respectively. The maximum strength (N_{max}) of 1380 kN was achieved at the end of testing and the corresponding EN1994 prediction (N_{EN}) is 1134.2 kN. If the values of N_{max} and N_{EN} are simply compared, it seems that EN1994 underestimates the strength of this specimen by 17.8%. However, N_u of this specimen should not be taken as its N_{max} since the axial strain (ε) of 0.24 corresponding to N_{max} obtained at the end of the testing is totally unrealistic for a member under axial compression. The specimen reached N_{EN} at an axial strain of 2.8%, which is still relatively high.

Following the definition by Tao et al. [20] and Uy et al. [22], the ultimate load-carrying capacity N_u in this paper is defined as the maximum or first peak load if the load is attained below an axial strain of 0.01; otherwise it is defined as the strength corresponding to a maximum strain limit of 0.01. For fibre reinforced polymer-confined concrete, a maximum compressive strain of 0.01 is also specified in ACI 440.2R [23] to prevent excessive cracking and the resulting loss of concrete integrity. Similarly, reaching an axial strain of 0.01 has been defined in ISO 834 [24] as a failure criterion for columns in fire. If the definition of N_u is applied, N_u–value of C7 corresponding to an axial strain of 0.01 is 1020 kN, which is 10.1% lower than N_{EN}, as shown in Fig. 1. This example demonstrates that care should be taken when using reported test results. Even when N_u is taken as N_{max}, EN1994 can sometimes overestimate the concrete confinement effect [25]. Thus, new models should be proposed to predict the compressive strength of CFST columns.

3. Finite element model

Apart from the above-mentioned limitations of test data, existing assembled test database also lacks uniformity regarding key parameters of material strengths and section slenderness because it was randomly assembled from numerous test results in the literature [26]. The results of code

comparison can be misleading if only the mean and standard deviation are checked for the predicted-to-measured strength ratios since most columns tested were small scale with normal material strength and section slenderness. More data outside the normal range of parameters is required to develop reliable design models. Meanwhile, test results of compressive stiffness and compressive strain corresponding to the ultimate strength of CFST stub columns were seldom reported in the literature. To develop accurate simplified models for these parameters, it is favourable to generate a large amount of data based on a reliable numerical model to cover a wide range of parameters. This will ensure the developed models are design-oriented but with theoretical background.

A FE model was successfully developed by Tao et al. [20] to simulate CFST stub columns using ABAQUS software [27]. The FE model has been rigorously verified by load–deformation curves of 142 circular, 154 square and 44 rectangular specimens, rather than just by reported ultimate strengths. The 340 curves are from 30 references and the majority of the references have received extensive citations. The parameter ranges for the circular specimens are: f_y=186-853 MPa, f_c'=18-185 MPa, D=60-450 mm, and D/t=17-221. For the rectangular specimens, the parameter ranges are: f_y=194-835 MPa, f_c'=13-164 MPa, H=60-500 mm, H/t=11-150, and H/B=1-2, where B is the width of a rectangular tube, and f_c' is the cylinder compressive strength of concrete. Obviously, the parameter ranges of both circular and rectangular test specimens are very broad and cover the current practical ranges.

In the FE modelling, the ratio of length L to diameter D (circular CFST) or cross-sectional height H (rectangular CFST) was chosen as 3 for a stub column. Shell elements S4R and solid elements C3D8R were used for the steel tube and core concrete, respectively. But when a steel tube has a small D/t (or H/t) ratio of 12 in the later parametric analysis, both the steel tube and core concrete

were simulated using solid elements C3D8R to avoid excessively thick shell elements. Surface-based interaction was used to model the concrete-steel tube interface. "Hard contact" in the normal direction was specified for the interface, whereas tangent contact was simulated using the Coulomb friction model with a specified friction coefficient of 0.6. The top and bottom surfaces of the steel tube and concrete were fixed against all degrees of freedom except for the axial displacement at the top end. The axial load was applied to the top end plate in a displacement control mode.

For rectangular CFST columns, an elastic-perfectly plastic model was adopted for the steel to better predict the descending branch of the load-deformation curve. But for circular CFST columns, the strain-hardening behaviour of steel was considered using the stress (σ)–strain (ε) model proposed by Tao et al. [28], which is expressed as follows

$$\sigma = \begin{cases} E_s \varepsilon & 0 \le \varepsilon < \varepsilon_y \\ f_y & \varepsilon_y \le \varepsilon < \varepsilon_p \\ f_u - (f_u - f_y) \cdot \left(\dfrac{\varepsilon_u - \varepsilon}{\varepsilon_u - \varepsilon_p} \right)^p & \varepsilon_p \le \varepsilon < \varepsilon_u \\ f_u & \varepsilon \ge \varepsilon_u \end{cases} \quad (1)$$

in which f_u is the ultimate strength of steel; E_s is the elastic modulus of steel; $\varepsilon_y = f_y/E_s$; ε_p is the strain at the beginning of strain hardening; ε_u is the ultimate strain of steel corresponding to f_u; and p is the strain-hardening exponent. Equations were proposed by Tao et al. [20,28] to determine f_u, ε_p, ε_u and p from f_y.

The concrete damaged plasticity model available in ABAQUS was used by Tao et al. [20] to simulate the confined concrete, where the following three-stage model was proposed to represent the strain hardening/softening rule of concrete confined by the steel tube:

$$\sigma = \begin{cases} \left[\dfrac{A'(\varepsilon/\varepsilon_{c0}) + B'(\varepsilon/\varepsilon_{c0})^2}{1 + (A'-2)(\varepsilon/\varepsilon_{c0}) + (B'+1)(\varepsilon/\varepsilon_{c0})^2}\right] \cdot f_c' & 0 < \varepsilon \le \varepsilon_{c0} \\ f_c' & \varepsilon_{c0} < \varepsilon \le \varepsilon_{cc} \\ f_r + (f_c' - f_r)\exp\left[-\left(\dfrac{\varepsilon - \varepsilon_{cc}}{\alpha}\right)^{\beta'}\right] & \varepsilon_{cc} < \varepsilon \end{cases} \quad (2)$$

where ε_{c0} and ε_{cc} are peak strains of the unconfined concrete and confined concrete, respectively; f_r is the residual stress of concrete; A', B', α and β' are material parameters [20].

More details of the FE model can be found in Tao et al. [20]. It has been proved that the developed three-dimensional FE model can accurately capture the local buckling of the steel tube and confinement to the concrete core, even when high-strength materials and/or thin-walled tubes are used.

The above FE model is used in this paper to generate simulation data with different material strengths and section slenderness ratios. A total of 499 CFST (270 circular and 229 rectangular) stub columns are analysed using various parameter combinations. Eight yield stress levels (f_y=175, 210, 300, 400, 500, 650, 800, 960 MPa) are chosen for the steel and five cylinder compressive strength levels (f_c'=20, 45, 70, 95, 120 MPa) are chosen for the concrete. For circular columns, the diameter-to-thickness ratio ranges from 12 to 150 (D/t=12, 33, 52, 75, 100, 127, 150). For rectangular columns, the height-to-width ratio varies at three levels (H/B=1, 1.5, 2) and the height-to-thickness ratio varies at five levels (H/t=12, 33, 52, 75, 100). In the analysis, the diameter or the width of the concrete core is kept at 400 mm, whereas the thickness of the steel tube is changed to obtain the required D/t ratio or H/t ratio.

4. Proposed model for compressive strength

4.1. Further evaluation of EN1994 model

Values of N_u are determined from numerical simulations according to the definition of N_u in Section

2. The obtained results are used to further evaluate the applicability of EN1994 in predicting N_u. Accordingly, EN1994 predictions (N_{EN}) are compared with the numerical results ($N_{u,FE}$) in Fig. 2. For all the circular columns, an average value (μ) of 1.040 is obtained for $N_{EN}/N_{u,FE}$ with a standard deviation (SD) of 0.049. For all the rectangular columns, the corresponding values of μ and SD are 1.002 and 0.060 respectively. If only these values are checked, the first impression is that EN1994 predicts the ultimate strength very well for both circular and rectangular columns. However, EN1994 can overestimate N_u of circular columns by up to 20% if the ratio of tf_y/Df_c' is very high. In fact, μ and SD of the $N_{EN}/N_{u,FE}$ ratio are 1.136 and 0.04 respectively for the 36 circular CFST samples with tf_y/Df_c' ratios equal to or greater than 0.5, as shown in Table 2. It should be mentioned that tf_y/Df_c' ratio indirectly reflects the concrete confinement effect. The larger the tf_y/Df_c' ratio, the higher the concrete confinement.

For a rectangular column, the width (B) and height (H) of the cross-section may be different. To account for the effect of non-uniform confinement in the rectangular column, an equivalent diameter D' recommended in ACI 440.2R-08 [23] is tentatively adopted in this paper to evaluate the concrete confinement effect:

$$D' = \sqrt{B^2 + H^2} \tag{3}$$

As shown in Table 3, the 229 analysed samples of rectangular columns can be classified into three groups according to their $tf_y/D'f_c'$ and H/t ratios. When $H/t \leq 100\sqrt{235/f_y}$ and $tf_y/D'f_c' < 0.707$, μ and SD of the $N_{EN}/N_{u,FE}$ ratio for the 155 samples are 0.986 and 0.030, respectively. These are normal rectangular CFST columns, and EN1994 [7] gives reasonably good strength predictions. But when the tubes are very thin ($H/t > 100\sqrt{235/f_y}$ and $tf_y/D'f_c' < 0.707$), μ and SD of the $N_{EN}/N_{u,FE}$ ratio for the 58 samples are 1.082 and 0.052, respectively. Clearly, unsafe predictions are given by EN1994 if the local buckling effect is not accounted for thin-walled rectangular CFST columns. In contrast,

the mean value of $N_{EN}/N_{u,FE}$ ratio is 0.922 for the 16 rectangular columns with compact sections ($tf_y/D'f_c' \geq 0.707$). It means that the concrete confinement effect has not been adequately considered by EN1994 for these columns with compact sections.

The above comparison further confirms that EN1994 can give unsafe or conservative predictions for the compressive strength of CFST columns. More accurate strength prediction models should be developed accordingly.

4.2. Proposed model

For a CFST under axial compression, the confined concrete is in a triaxial stress state and the steel is in a biaxial state after the development of "composite action" between the steel tube and concrete. The confinement to concrete can lead to the increase of its compressive strength, whereas the development of tensile hoop stresses in the steel tube reduces its load-carrying capacity in the axial direction. This mechanism has been well established [29]. Meanwhile, the load-carrying capacity of the steel tube will decrease further if local buckling of the tube occurs prior to the ultimate state. Considering the contributions from the steel tube and concrete, a simple superposition model is proposed as follows to predict the ultimate strength for both circular and rectangular CFST columns:

$$N_u = N_a + N_c = \eta_a f_y A_s + \eta_c f_c' A_c \tag{4}$$

where N_a and N_c are the strength contributions from the steel tube and concrete, respectively; A_s and A_c are the cross-sectional areas of the steel tube and core concrete, respectively; η_a is a reduction factor (smaller than 1) for the strength contribution of the steel tube to consider the influence of concrete confinement and possible local buckling of the steel tube; and η_c is an amplification factor (larger than 1) to account for the increased strength of concrete due to the confinement effect. The derivation of η_a and η_c is presented in the following subsections.

4.2.1. Circular CFST columns

At the ultimate state, the loads carried by the steel tube (N_a) and concrete (N_c) can be determined from the numerical analysis of a CFST stub column. To avoid the end effects, N_a and N_c are derived from the mid-height of the column. Based on Eq. (4), the factors of η_a and η_c can be determined as: $\eta_a=N_a/f_yA_s$ and $\eta_c=N_c/f_c'A_c$.

Parametric analysis indicates that η_a is mainly affected by the D/t ratio of the steel tube and its yield stress f_y, whereas the concrete strength has little influence on η_a. In general, η_a increases with increasing f_y or decreasing D/t ratio, as depicted in Fig. 3. When f_y increases or D/t ratio decreases, the concrete is under increased confinement. However, the ratio of hoop tensile stress to the yield stress of the steel tube decreases, leading to increased η_a.

A nonlinear regression is performed and Eq. (5) is proposed to predict η_a for circular CFST columns:

$$\eta_a = 0.95 - 12.6 f_y^{-0.85} \ln(0.14D/t) \tag{5}$$

where the unit for f_y is MPa. As shown in Fig. 4, the coefficient of determination R^2 is 0.932, indicating a very good fitting model. The data points shown in this figure are obtained from FE analysis.

The amplification factor η_c for the concrete is mainly affected by tf_y/Df_c', D/t and f_c', as shown in Fig. 5. Increasing tf_y/Df_c' or decreasing D/t or f_c' leads to increasing concrete confinement. As can be seen from Fig. 5(a) and (b), η_c decreases dramatically as D/t or f_c' increases initially. Then η_c becomes stable at a value larger than 1. In contrast, η_c increases almost linearly with increasing tf_y/Df_c' ratio, as shown in Fig. 5(c). Regression analysis indicates that η_c may be expressed as a function of tf_y/Df_c' ratio only. However, if D/t and f_c' are introduced as additional terms, a better

model can be produced for η_c as shown in Fig. 6, where the value of R^2 is 0.996. The equation to predict η_c is given as follows:

$$\eta_c = 0.99 + \left[5.04 - 2.37\left(\frac{D}{t}\right)^{0.04}(f_c')^{0.1}\right]\left(\frac{tf_y}{Df_c'}\right)^{0.51} \quad (6)$$

where the unit of f_c' is MPa.

4.2.2. Rectangular CFST columns

Similar to circular CFST columns, the η_a factor for rectangular CFST columns is mainly affected by the D'/t ratio and f_y. Since thin-walled rectangular tubes are very susceptible to local buckling, η_a decreases dramatically after reaching a certain limit, as shown in Fig. 7. This is in contrast to circular CFST columns as shown in Fig. 3(a), since local buckling is less likely to occur or occurs at a much later stage for circular tubes. Based on regression analysis, the following equation is proposed to predict η_a for the rectangular CFST columns:

$$\eta_a = 0.91 + 7.31\times10^{-5} f_y - \left(1.28\times10^{-6} + 2.26\times10^{-8} f_y\right)\left(\frac{D'}{t}\right)^2 \quad (7)$$

where the unit of f_y is MPa. By comparing with simulation data, the accuracy of the proposed model for η_a can be seen in Fig. 8.

For rectangular CFST columns, it is well known that only concrete in the core and at the corners is effectively confined while the confinement to the rest is negligible. The concept of effective confining area is often used to account for this effect. Based on this concept, Lam and Teng [30] proposed an equivalent confining coefficient k_s, which is adopted in this paper:

$$k_s = \frac{1}{3}\left(\frac{b}{h}\right)^2 = \frac{1}{3}\left(\frac{B-2t}{H-2t}\right)^2 \quad (8)$$

where b and h are the width and height of the rectangular concrete core. When h/b increases from 1

to 2, k_s decreases from 0.333 to 0.083.

Parametric analysis indicates that η_c of rectangular CFST columns is mainly affected by the $tf_y/D'f_c'$ ratio, as shown in Fig. 9(a). This trend is similar to that observed in Fig. 5(c) for circular CFST columns. Meanwhile, it is found that η_c is also slightly affected by k_s, as well as by f_y as shown in Fig. 9(b) and (c). However, for rectangular CFST columns with very compact section (D'/t=17), the influence of f_y becomes more pronounced. Based on regression analysis, Eq. (9) is proposed to predict η_c, which is a function of k_s, f_y and $tf_y/D'f_c'$:

$$\eta_c = 0.98 + 29.5\left(f_y\right)^{-0.48} k_s^{\,0.2}\left(\frac{tf_y}{D'\,f_c'}\right)^{1.3} \tag{9}$$

where the unit for f_y is MPa. The accuracy of the proposed model for η_c can be seen from the comparison with numerical data shown in Fig. 10.

4.3. Prediction accuracy

Calculated ultimate strengths (N_{uc}) from Eq. (4) are compared with FE predictions ($N_{u,FE}$) of circular and rectangular CFST columns, as shown in Fig. 11. Very good agreement is achieved between N_{uc} and $N_{u,FE}$ for all the 499 numerical examples. This is in contrast to the EN1994 predictions as shown in Fig. 2. For circular CFST stub columns, the improvement of the current model against EN1994 model can be further seen from the comparisons shown in Table 2 for both groups of samples (tf_y/Df_c'<0.5 and tf_y/Df_c'≥0.5). Similarly, for rectangular CFST stub columns, the improvement of the current model against EN1994 model can be found from the comparisons shown in Table 3 for three groups of samples ($tf_y/D'f_c'$<0.707 and $H/t > 100\sqrt{235/f_y}$; $tf_y/D'f_c'$<0.707 and $H/t \le 100\sqrt{235/f_y}$; and $tf_y/D'f_c'$≥0.707).

Calculated strengths of N_{uc} from Eq. (4) are further compared with test strengths (N_{ue}) retrieved

from the load–deformation curves of 118 circular CFST columns and 177 rectangular CFST columns as shown in Figs. 12(a) and 13(a), respectively. The majority of the curves were collected by Tao et al. [20] except those of four square high strength CFST specimens recently presented by Khan et al. [31]. The load–deformation curves of 24 circular columns and 21 square columns collected by Tao et al. [20] are not used in this paper since only load versus axial shortening curves were reported. The end effects caused a significant reduction in initial compressive stiffness, resulting in significant errors in determining N_u from the load–axial shortening curves.

As expected, Figs. 12(a) and 13(a) show obvious variation in the predictions due to the unavoidable experimental errors. However, compared to the EN1994 predictions shown in Figs. 12(b) and 13(b), obvious improvement in predictions can still be identified for the proposed simplified model. Meanwhile, the current model is also much simpler than the EN1994 model.

5. Proposed model for compressive stiffness

Steel exhibits a sensibly linear stress–strain relation before reaching its elastic limit. But the development of microcracks in concrete leads to the decrease of the secant modulus with an increase in stress [32]. In practice, the modulus of elasticity for concrete (E_c) is often defined as the secant modulus corresponding to $0.4f_c'$. Due to the concrete cracking, the secant compressive stiffness of CFST columns also decreases with increasing compressive load. Huo et al. [33] and Yang et al. [34] defined the compressive stiffness (EA) as the secant stiffness corresponding to the column strength of $0.4N_u$. This definition is also adopted in this paper to derive EA from N–ε curves.

Values of compressive stiffness $(EA)_{FE}$ retrieved from the numerical examples are compared in Fig. 14 with calculated stiffness based on superposition $[(EA)_s=E_sA_s+E_cA_c]$. As can be seen, only when tf_y/Df_c' or $tf_y/D'f_c'$ is very small, $(EA)_{FE}$ is close to $(EA)_s$. When tf_y/Df_c' is greater than 0.3 for circular

CFST columns or $tf_y/D'f_c'$ is greater than 0.35 for rectangular CFST columns, $(EA)_{FE}$ is often smaller than $(EA)_s$. From numerical results, it is found that the steel tube normally remains elastic when the axial load reaches $0.4N_u$. However, the concrete stress has exceeded $0.4f_c'$ due to the concrete confinement. If the confinement is strong, significant reduction in concrete stiffness might occur. Therefore, a correction factor κ_c is introduced for the concrete stiffness and Eq. (10) is proposed to predict *EA*.

$$EA = E_s A_s + \kappa_c E_c A_c \tag{10}$$

5.1. Determining κ_c for circular CFST columns

From Eq. (10), κ_c can be expressed as $(EA–E_sA_s)/E_cA_c$. Accordingly, κ_c can be calculated once *EA* is determined from numerical simulation. Parametric analysis indicates that κ_c is mainly affected by the D/t ratio and tf_y/Df_c' for circular CFST columns. As exhibited in Figs. 14(a) and 15(a), κ_c decreases with increasing tf_y/Df_c' or decreasing D/t ratio. This confirms that the reduction in concrete stiffness increases with an increase in concrete confinement.

Based on regression analysis, the following equation is proposed to determine κ_c for circular CFST columns:

$$\kappa_c = \left(\frac{D}{t}\right)^{0.004} + \left(\frac{tf_y}{Df_c'}\right)^{1.5}\left[56.8 - 56.3\left(\frac{D}{t}\right)^{0.004}\right] \le 1 \tag{11}$$

where the units for f_y and f_c' are MPa. The coefficient of determination R^2 is 0.886 for the κ_c regression. As can be seen from Fig. 16, the predicted values of κ_c agree very well with numerical data.

5.2. Determining κ_c for rectangular CFST columns

Similar to circular CFST columns, κ_c decreases with increasing $tf_y/D'f_c'$ or decreasing D'/t ratio for rectangular CFST columns, as can be seen from Figs. 14(b) and 15(b). Based on regression analysis,

the following formula is proposed to calculate κ_c for rectangular CFST columns:

$$\kappa_c = \left(\frac{D'}{t}\right)^{0.003} + \left(\frac{tf_y}{D' f_c'}\right)^{2.3}\left[103.12 - 102.26\left(\frac{D'}{t}\right)^{0.003}\right] \le 1 \quad (12)$$

where the units for f_y and f_c' are MPa. The coefficient of determination R^2 is 0.935 for the κ_c regression. The comparison shown in Fig. 17 demonstrates that the predicted values of κ_c have a good agreement with the simulated results.

5.3. Prediction accuracy

The predicted values of compressive stiffness $(EA)_c$ using Eq. (10) are compared with FE predictions $(EA)_{FE}$, as shown in Fig. 18. For the samples of 270 circular CFST columns, the average value (μ) and standard deviation coefficient (SD) of $(EA)_c/(EA)_{FE}$ are 1.000 and 0.012, respectively. Meanwhile, for the samples of 229 rectangular CFST columns, μ and SD of $(EA)_c/(EA)_{FE}$ are 0.997 and 0.010, respectively. Thus, it is confirmed that the proposed simplified model for compressive stiffness has very good accuracy.

6. Proposed model for compressive strain corresponding to the ultimate strength

The compressive strain (ε_c) corresponding to the ultimate strength to some extent reflects the deformation ability and ductility of a CFST stub column, which may be of interest to the designers. ε_c-values obtained from numerical simulation ($\varepsilon_{c,FE}$) are used to analyse the influence of different parameters. It is found that $\varepsilon_{c,FE}$ normally increases with increasing f_y and decreasing f_c' or D/t (or D'/t) ratio, as shown in Figs. 19 and 20. This indicates the increasing influence of concrete confinement. The higher the concrete confinement, the larger the compressive strain ε_c.

For rectangular CFST columns, it is also observed from Fig. 20(b) that $\varepsilon_{c,FE}$ increases with an increase in f_c' when the D'/t ratio is 106.1 or 141.4. This is owing to the fact that the concrete

confinement is very moderate in thin-walled rectangular CFST columns. In this case, ε_c of a composite column is mainly determined by the peak strain (ε_0) corresponding to the ultimate strength of the unconfined concrete, which increases with increasing f_c' [20].

Based on nonlinear regression analysis, Eq. (13a) and (13b) are proposed to predict ε_c for circular and rectangular CFST stub columns, respectively:

$$\varepsilon_c = 3000 - 10.4 f_y^{1.4} (f_c')^{-1.2} \left[0.73 - 3785.8 (D/t)^{-1.5}\right] \le 10000\mu\varepsilon \quad \text{for circular CFST} \tag{13a}$$

$$\varepsilon_c = 2300 + 31.2 f_c'^{0.7} + \left(2.32\times10^4 - 3.88\times10^6 f_c'^{-1.8}\right)\left(\frac{t f_y}{D' f_c'}\right)^2 \quad \text{for rectangular CFST} \tag{13b}$$

where the units for f_y and f_c' are MPa.

Fig. 21 compares the predicted compressive strains ($\varepsilon_{c,c}$) from Eq. (13) with the FE predictions ($\varepsilon_{c,FE}$). For the 270 circular CFST samples, the average value (μ) and standard deviation (SD) of the $\varepsilon_{c,c}/\varepsilon_{c,FE}$ ratio are 0.999 and 0.052, respectively; whereas the corresponding values are 0.999 and 0.053, respectively, for the 229 rectangular CFST samples. Due to the influence of possible local buckling, it seems that the predictions for rectangular columns are less accurate than those for circular columns. Despite this, the predictions of the simplified model for the ultimate strain are still reasonable.

7. Capacity factor calibration

To ensure safety and serviceability of structures, it is required by design codes to apply safety factors to materials or the resistance equations. Accordingly, capacity reduction factors for steel (ϕ) and concrete (ϕ_c) are introduced into Eq. (4) to calculate the nominal section capacity (N_{us}):

$$N_{us} = \phi \eta_a f_y A_s + \phi_c \eta_c f_c' A_c \tag{14}$$

In the Australian code AS 4100 [6], the specified values are 0.9 and 0.6 for ϕ and ϕ_c, respectively.

Since Eq. (14) is different from that in AS 4100 for predicting N_{us}, it is necessary to recalibrate the capacity reduction factors in this equation.

Kang et al. [26] recently recalibrated the capacity reduction factors in AS 4100 used for CFST stub columns based on the statistical method proposed by Johnson and Huang [35]. This method calibrates multiple capacity factors extensively applying the theoretical background of the statistical method given in EN 1990 Annex D.8 [36]. This method provides procedures for calibrating multiple capacity factors as the ratio of the design resistance to the nominal resistance utilising experimental data.

The detailed procedure presented by Kang et al. [26] is followed in this paper. The target reliability index for both resistance and load effects can be taken as 3.8 (equivalent to the probability of the actual strength lower than the design strength of 0.0012). To consider the resistance effect separately from the load effect, a FORM sensitivity factor of 0.8 is multiplied to the target reliability index, and the reliability index for resistance only is calculated as $\beta = 3.8 \times 0.8 = 3.04$ [37]. The test ultimate strengths (N_{ue}) retrieved from the load–deformation curves of 118 circular CFST columns and 177 rectangular CFST columns shown in Figs. 12 and 13 are used for the calibration. In the calibration process, it is assumed that the mean values of the input parameters (material strengths and cross-sectional dimensions) are taken as the mean measured values from the tests, and the coefficients of variation of the input parameters are obtained from the design codes [6,38-41], as presented in Table 4.

Fig. 22 presents the calibrated capacity reduction factors (ϕ or ϕ_c) as a function of target reliability index (β). Values of both ϕ and ϕ_c decrease with increasing β. When the target reliability index is taken as 3.04, the capacity reduction factors (ϕ and ϕ_c) for circular CFST stub columns are 0.90 and

0.83; whereas those for rectangular CFST columns are 0.83 and 0.78, as shown in Table 5. As can be seen, the capacity reduction factors for rectangular columns are smaller than those of circular columns due to the larger scatter of the predictions using Eq. (4) for rectangular columns, as shown in Fig. 13. In design, smaller values of 0.83 and 0.78 may be used for ϕ and ϕ_c, respectively, in all cases.

To clearly demonstrate the influence of using new capacity factors for the proposed equations rather than those specified in AS 4100 [6], the steel capacity factor (ϕ) may be fixed to a constant value of 0.9 as specified in AS 4100, and the concrete capacity factor (ϕ_c) can be calibrated using the same procedure. The obtained results are shown in Fig. 23. When β is taken as 3.04, the obtained values of ϕ_c are 0.83 and 0.74 for circular and rectangular columns, respectively. For design purposes, a constant ϕ_c of 0.74 may be used for all CFST columns, and this value is higher than the value of 0.6 specified in AS 4100 [6]. Clearly, higher nominal section capacities will be obtained for CFST stub columns if the proposed capacity reduction factors are used for steel and concrete. It should be noted that the strength predictions when ϕ and ϕ_c are taken as 0.83 and 0.78 respectively are virtually the same as those when ϕ is taken as 0.9 and ϕ_c as 0.74. The errors are within 5%.

8. Conclusions

This paper focused on the predictions of compressive strength and corresponding strain as well as compressive stiffness of circular and rectangular concrete-filled steel stub columns subjected to axial compression. Through the current investigation, the following conclusions can be obtained:

(1) Existing design codes have various limitations in predicting the compressive strength. The new simplified models proposed in this paper cover a wide range of parameters: diameter-to-thickness ratio (D/t=12-150); width-to-thickness ratio (B/t=12-100); height-to-width ratio (H/B=1-2); yield

stress of steel (f_y=175-960 MPa) and concrete cylinder compressive strength (f_c'=20-120 MPa). The effects of concrete confinement and possible local buckling of the steel tube have been implicitly included in the models, which simplifies the strength calculation.

(2) Based on numerical data, simplified models have been proposed for the predictions of compressive stiffness and compressive strain corresponding to the ultimate strength. These models can be used in structural analysis and to assist the evaluation of ductility and deformation capacity.

(3) To assist the use of the new strength prediction models, capacity reduction factors for the steel and concrete materials have been recalibrated to achieve a target reliability index of 3.04 when considering resistance effect only. The capacity reduction factors can be taken as 0.83 and 0.78 for the steel and concrete, respectively.

Acknowledgements

This work is supported by the Australian Research Council Discovery Project (Grant No: DP170100001). It has also been supported by the China Scholarship Council.

References

[1] N.E. Shanmugam, B. Lakshmi, State of the art report on steel-concrete composite columns, Journal of Constructional Steel Research, 57 (10) (2001) 1041–1080.

[2] L.H. Han, Tests on stub columns of concrete-filled RHS sections, Journal of Constructional Steel Research, 58 (3) (2002) 353–372.

[3] L.H. Han, W. Li, R. Bjorhovde, Developments and advanced application of concrete-filled steel tubular (CFST) structures: Members, Journal of Constructional Steel Research, 100 (9) (2014) 211–228.

[4] Z. Tao, T.Y. Song, B. Uy, L.H. Han, Bond behavior in concrete-filled steel tubes, Journal of Constructional Steel Research, 120 (2016) 81–93.

[5] Architectural Institute of Japan (AIJ), Recommendations for design and construction of concrete filled steel tubular structures, AIJ, Tokyo, Japan, 1998.

[6] Standards Australia, Bridge design, Part 6: Steel and composite construction, AS5100.6–2004,

Sydney, Australia, 2004.

[7] European Committee for Standardization (CEN), Design of composite steel and concrete structures - part 1-1: general rules and rules for buildings, EN 1994-1-1 Eurocode 4, Brussels, 2004.

[8] American Institute of Steel Construction (AISC), Specification for structural steel buildings, AISC 360-10, Chicago (IL), 2010.

[9] American Concrete Institute, Building code requirements for structural concrete and commentary, ACI 318-11, Farmington Hills, MI, 2011.

[10] DBJ 13-51-2010, Development of Fujian Province, Technical specification for concrete-filled steel tubular structures, Department of Housing and Urban, 2010 [in Chinese].

[11] Z.H. Lu, Y.G. Zhao, Suggested empirical models for the axial capacity of circular CFT stub columns, Journal of Constructional Steel Research, 66 (6) (2010) 850–862.

[12] F. Aslani, B. Uy, Z. Tao, F. Mashiri, Predicting the axial load capacity of high-strength concrete filled steel tubular columns, Steel and Composite Structures, 19 (4) (2015) 967–993.

[13] Z. Tao, B. Uy, L.H. Han, S.H. He, Design of concrete-filled steel tubular members according to the Australian Standard AS 5100 model and calibration, Australian Journal of Structural Engineering, 8 (3) (2008) 197–214.

[14] A. Kuranovas, D. Goode, A.K. Kvedaras, S. Zhong, Load–bearing capacity of concrete-filled steel columns, Journal of Civil Engineering and Management, 15 (1) (2009) 21–33.

[15] E.M. Güneyisi, A. Gültekin, K. Mermerdaş, Ultimate capacity prediction of axially loaded CFST short columns, International Journal of Steel Structures, 16 (1) (2016) 99–114.

[16] C. Chaseling, Star attraction, Modern steel construction, 44 (12) (2004) 36–42.

[17] J.Y.R. Liew, M.X. Xiong, D.X. Xiong, Design of high strength concrete filled tubular columns for tall buildings, International Journal of High-Rise Buildings, 3 (3) (2014) 215–221.

[18] L.H. Han, G.H. Yao, X.L. Zhao, Tests and calculations of hollow structural steel (HSS) stub columns filled with self-consolidating concrete (SCC), Journal of Constructional Steel Research, 61 (9) (2005) 1241–1269.

[19] F.X. Ding, Z.W. Yu, Y. Bai, Y.Z. Gong, Elasto-plastic analysis of circular concrete-filled steel tube stub columns, Journal of Constructional Steel Research, 67 (10) (2011) 1567–1577.

[20] Z. Tao, Z.B. Wang, Q. Yu, Finite element modelling of concrete-filled steel stub columns under axial compression, Journal of Constructional Steel Research, 89 (10) (2013) 121–131.

[21] G. Giakoumelis, D. Lam, Axial capacity of circular concrete-filled tube columns, Journal of Constructional Steel Research, 60 (7) (2004) 1049–1068.

[22] B. Uy, Z. Tao, L.H. Han, Behaviour of short and slender concrete-filled stainless steel tubular

columns, Journal of Constructional Steel Research, 67 (3) (2011) 360–378.

[23] American Concrete Institute (ACI), Guide for the design and construction of externally bonded FRP systems for strengthening concrete structures, ACI 440.2R-08, USA, 2008.

[24] International Organization for Standardization (ISO), Fire-resistance tests—elements of building construction-part 1: general requirements, ISO 834-1, Geneva, 1999.

[25] W.L.A. de Oliveira, S. De Nardin, A.L.H. de Cresce El, M.K. El Debs, Influence of concrete strength and length/diameter on the axial capacity of CFT columns, Journal of Constructional Steel Research, 65 (12) (2009) 2103–2110.

[26] W.H. Kang, B. Uy, Z. Tao, S. Hicks, Design strength of concrete-filled steel columns, Advanced Steel Construction, 11 (2) (2015) 165–184.

[27] ABAQUS, ABAQUS standard user's manual, Version 6.9, Dassault Systèmes Corp., Providence, RI (USA), 2009.

[28] Z. Tao, X.Q. Wang, B. Uy, Stress–strain curves of structural and reinforcing steels after exposure to elevated temperatures, J Mater Civ Eng, 25(9) (2013) 1306–1316.

[29] M. Johansson, K. Gylltoft, Mechanical behavior of circular steel-concrete composite stub columns, Journal of Structural Engineering, ASCE, 128 (8) (2002) 1073–1081.

[30] L. Lam, J.G. Teng, Design-oriented stress–strain model for FRP-confined concrete in rectangular columns, Journal of Reinforced Plastics and Composites, 22 (13) (2003) 1149–1186.

[31] M. Khan, B. Uy, Z. Tao, F. Mashiri, Concentrically loaded short high strength composite columns, Pacific Structural Steel Conference, Singapore, 2013.

[32] A.M. Neville, Properties of concrete, Florida, United States: Addison-Wesley Longman, Limited, 2011.

[33] J.S Huo, G.W. Huang, Y. Xiao, Effects of sustained axial load and cooling phase on post-fire behaviour of concrete-filled steel tubular stub columns, Journal of Constructional Steel Research, 65 (8) (2009) 1664–1676.

[34] Y.F. Yang, K. Cao, T.Z. Wang, Experimental behavior of CFST stub columns after being exposed to freezing and thawing, Cold Regions Science and Technology. 89 (2013) 7–21.

[35] R.P. Johnson, D. Huang, Statistical calibration of safety factors for encased composite columns, Composite Construction in Steel and Concrete III, ASCE, New York, USA, 1997, pp. 380–391.

[36] European Committee for Standardization (CEN), Basis of structural design, EN 1990: 2002 Eurocode, Brussels, 2002.

[37] International Organization for Standardization (ISO), ISO 2394:1998 General principles on reliability for structures, Geneva, Switzerland, 1998.

[38] Joint Committee on Structural Safety (JCSS), JCSS probabilistic model code,

http://www.jcss.byg.dtu.dk/, 2001.

[39] Standards Australia International Ltd., Concrete structures, AS 3600:2009, New South Wales, Australia, 2009.

[40] Standards New Zealand (NZS), Specification for concrete production, NZS 3104: 2003, Wellington, New Zealand, 2003.

[41] Standards Australia/Standards New Zealand (AS/NZS), Cold-formed structural steel hollow sections, AS/NZS 1163: 2009, Sydney, Australia, 2009.

Captions for Figures

Fig. 1. Comparison between N_{EN} and N_u for a typical column C7 [21] with compact section.

Fig. 2. Comparison between $N_{u,FE}$ and N_{EN}.

Fig. 3. Effects of f_y and D/t ratio on η_a of circular CFST columns.

Fig. 4. η_a of circular CFST columns as a function of f_y and D/t ratio.

Fig. 5. Effects of different parameters on η_c of circular CFST columns.

Fig. 6. η_c of circular CFST columns as a function of f_c', D/t ratio and tf_y/Df_c'.

Fig. 7. Effects of D'/t ratio on η_a of rectangular CFST columns.

Fig. 8. η_a of rectangular CFST columns as a function of f_y and D'/t ratio.

Fig. 9. Effects of different parameters on η_c of rectangular CFST columns.

Fig. 10. η_c of rectangular CFST columns as a function of k_s, f_y and $tf_y/D'f_c'$.

Fig. 11. Comparison between N_{uc} and $N_{u,FE}$ of CFST columns.

Fig. 12. Comparison between N_{uc}, N_{EN} and N_{ue} of circular CFST columns.

Fig. 13. Comparison between N_{uc}, N_{EN} and N_{ue} of rectangular CFST columns.

Fig. 14. Comparison between $(EA)_{FE}$ and $(EA)_s$.

Fig. 15. Effects of D/t (or D'/t) ratio on concrete stiffness of CFST columns.

Fig. 16. Prediction accuracy of κ_c for circular CFST columns.

Fig. 17. Prediction accuracy of κ_c for rectangular CFST columns.

Fig. 18. Comparison between $(EA)_c$ and $(EA)_{FE}$ of CFST columns.

Fig. 19. Effects of f_y, f_c' and D/t ratio on compressive strains of circular CFST columns.

Fig. 20. Effects of f_y, f_c' and D'/t ratio on compressive strains of rectangular CFST columns.

Fig. 21. Comparison between $\varepsilon_{c,c}$ and $\varepsilon_{c,FE}$ of CFST columns.

Fig. 22. Capacity factor versus reliability index for CFST columns.

Fig. 23. Concrete capacity factor versus reliability index when ϕ is taken as 0.9.

Captions for Tables

Table 1 Strength prediction methods and related limitations.

Table 2 Strength comparison between FE and simple calculations for circular CFST columns.

Table 3 Strength comparison between FE and simple calculations for rectangular CFST columns.

Table 4 COV of input parameters.

Table 5 Reliability indices when the target reliability index is taken as 3.04.

Figures

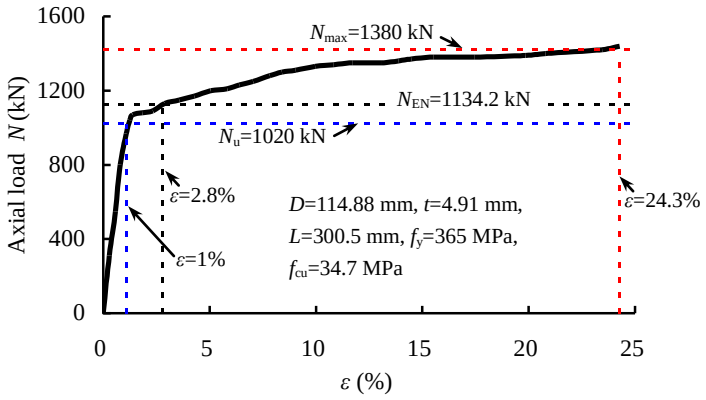

Fig. 1. Comparison between N_{EN} and N_u for a typical column C7 [21] with compact section.

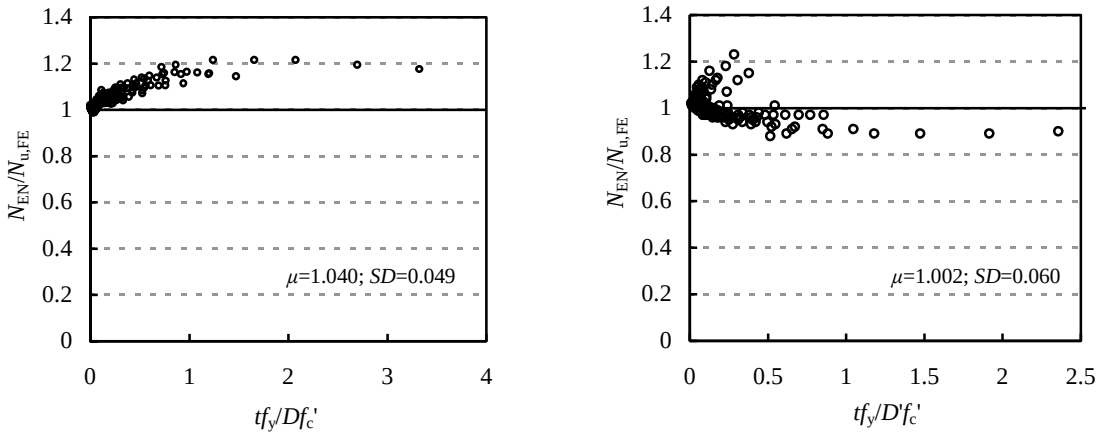

(a) Circular CFST (b) Rectangular CFST

Fig. 2. Comparison between $N_{u,FE}$ and N_{EN}.

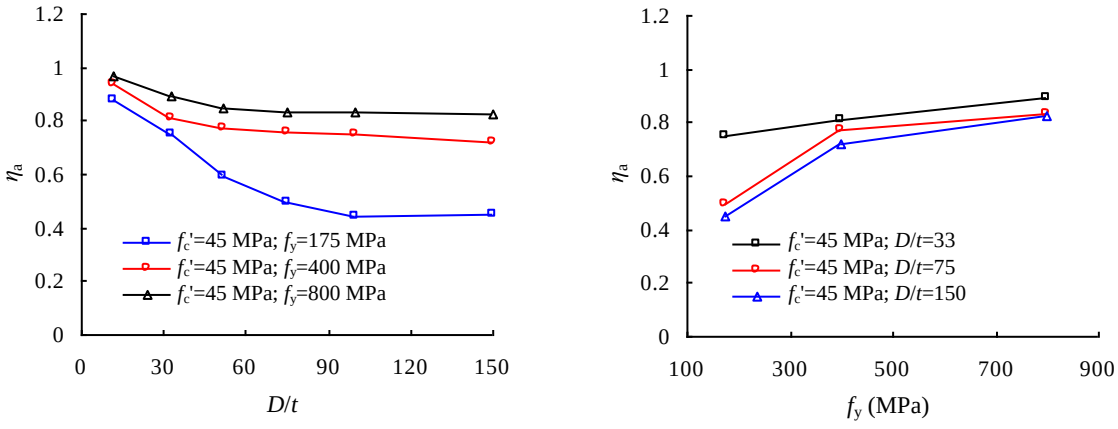

(a) (b)

Fig. 3. Effects of f_y and D/t ratio on η_a of circular CFST columns.

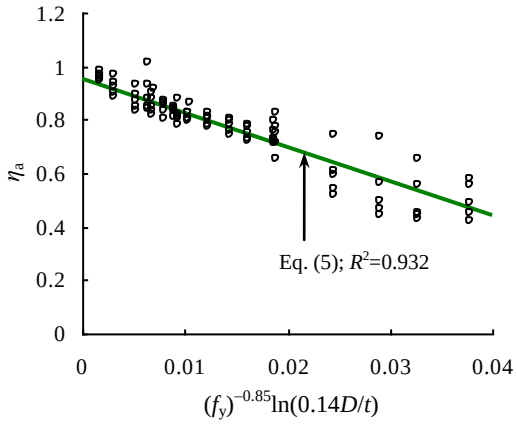

Fig. 4. η_a of circular CFST columns as a function of f_y and D/t ratio.

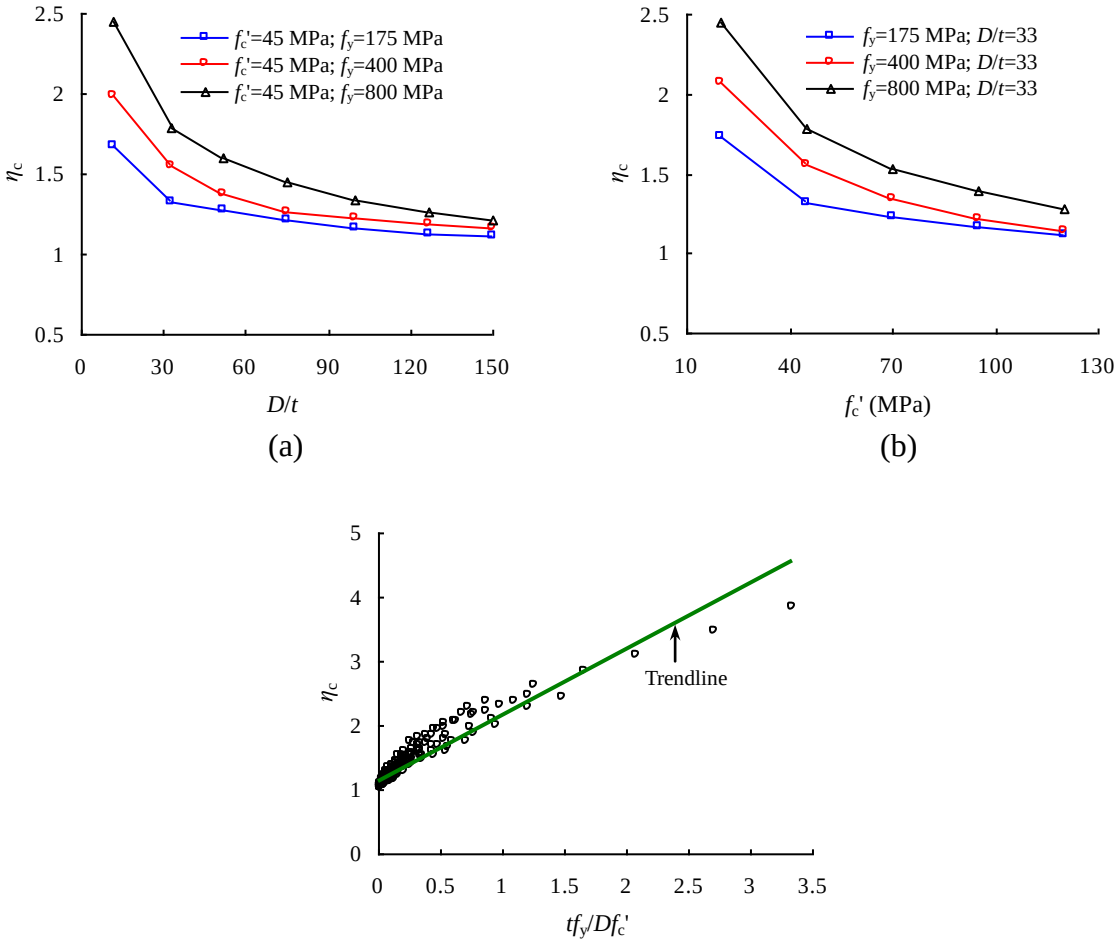

Fig. 5. Effects of different parameters on η_c of circular CFST columns.

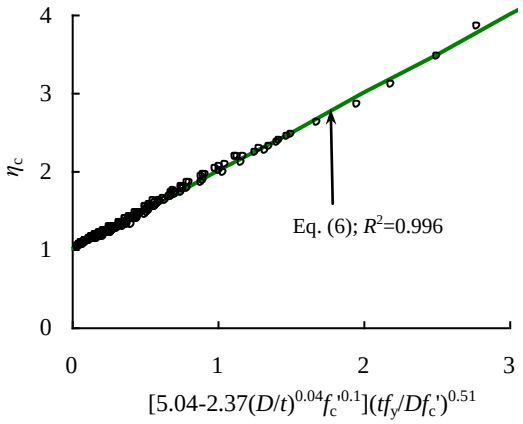

Fig. 6. η_c of circular CFST columns as a function of f_c', D/t ratio and tf_y/Df_c'.

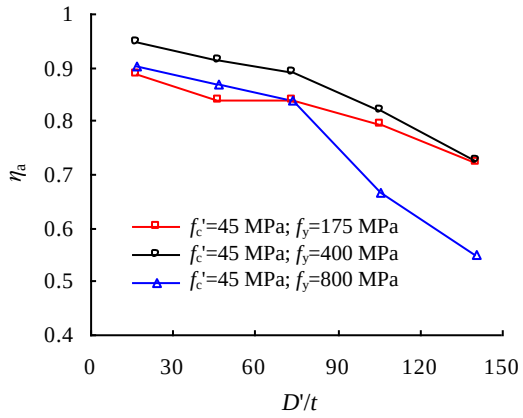

Fig. 7. Effects of D'/t ratio on η_a of rectangular CFST columns.

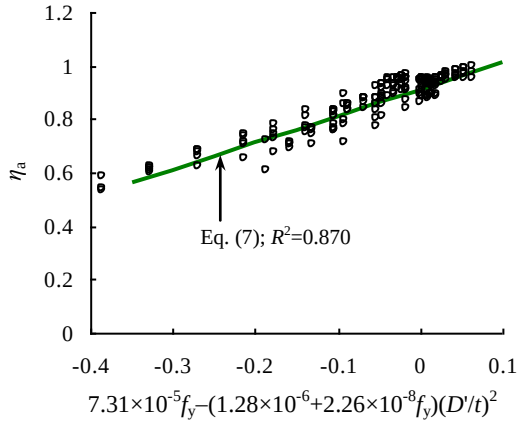

Fig. 8. η_a of rectangular CFST columns as a function of f_y and D'/t ratio.

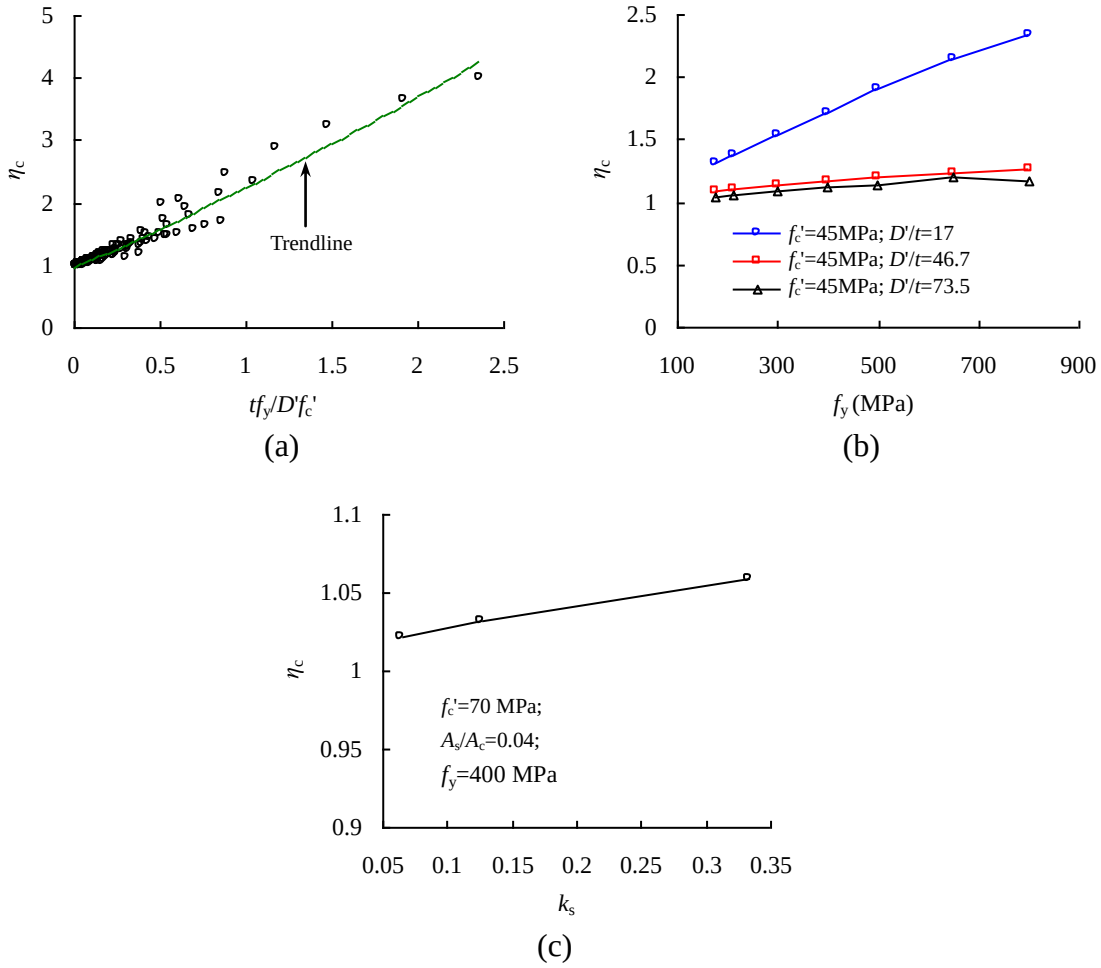

Fig. 9. Effects of different parameters on η_c of rectangular CFST columns.

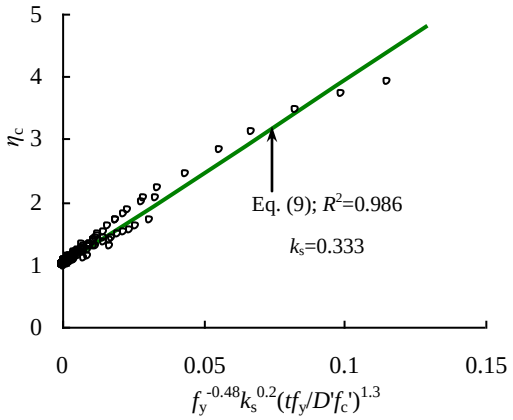

Fig. 10. η_c of rectangular CFST columns as a function of k_s, f_y and $tf_y/D'f_c'$.

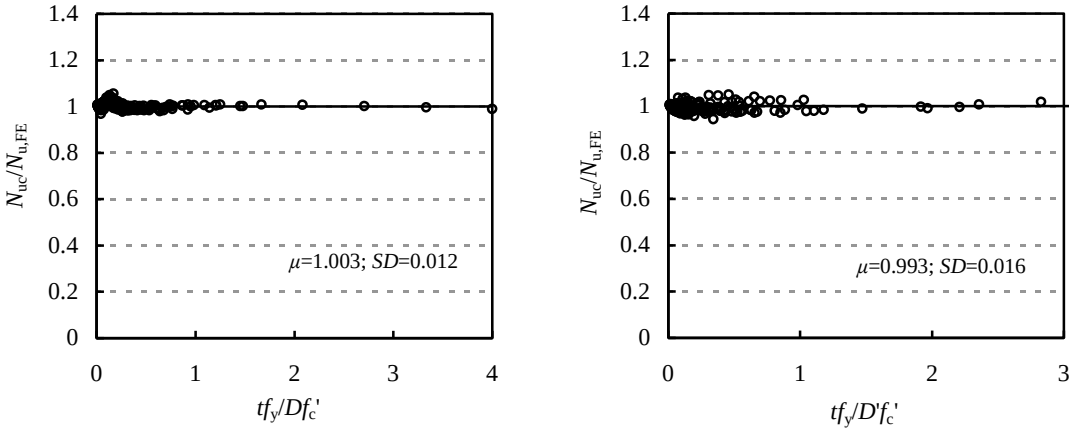

(a) Circular CFST (b) Rectangular CFST

Fig. 11. Comparison between N_{uc} and $N_{u,FE}$ of CFST columns.

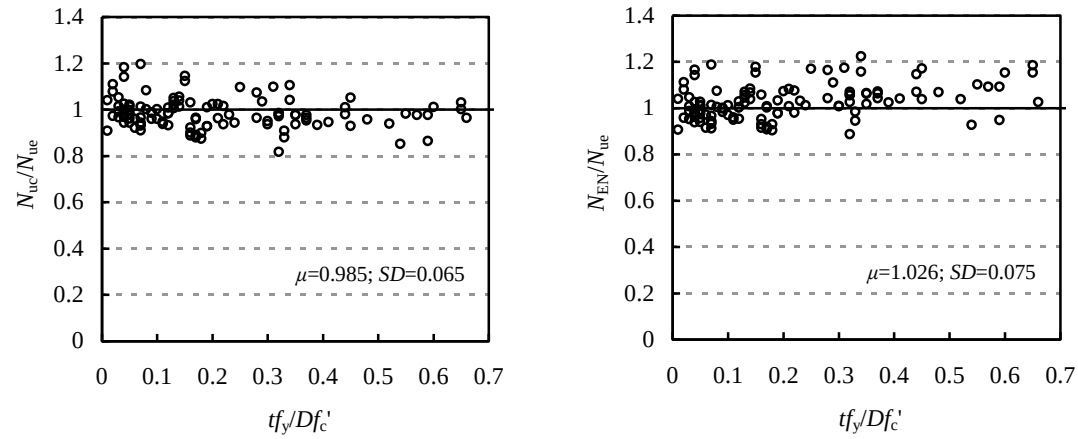

(a) Current model (b) EN1994 model

Fig. 12. Comparison between N_{uc}, N_{EN} and N_{ue} of circular CFST columns.

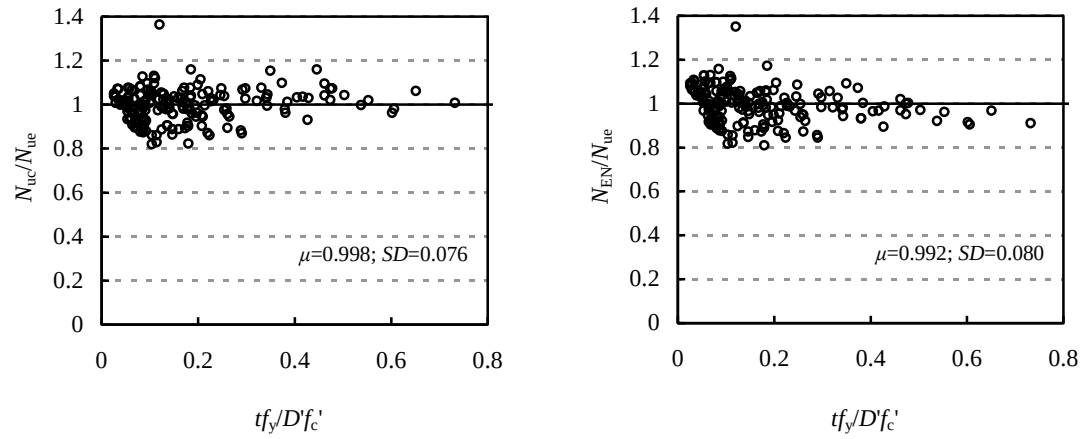

(a) Current model (b) EN1994 model

Fig. 13. Comparison between N_{uc}, N_{EN} and N_{ue} of rectangular CFST columns.

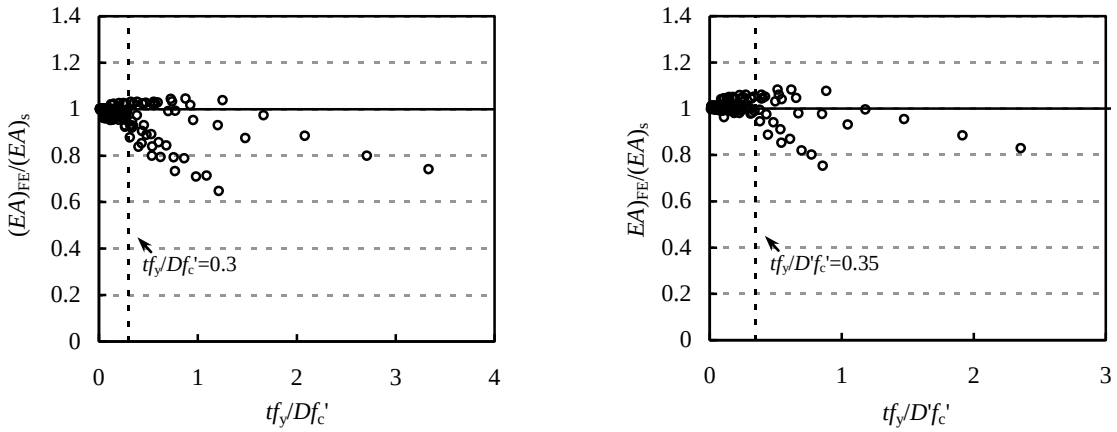

(a) Circular CFST (b) Rectangular CFST

Fig. 14. Comparison between $(EA)_{FE}$ and $(EA)_s$.

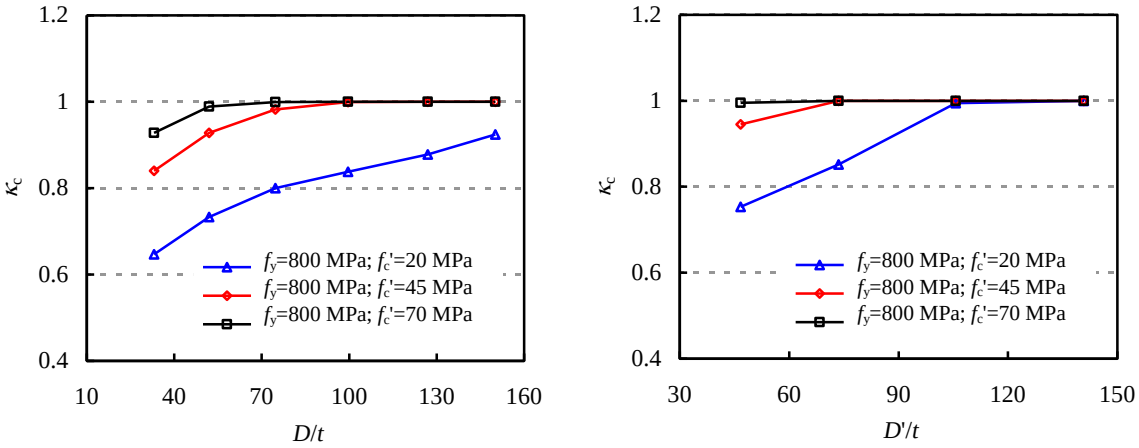

(a) Circular CFST (b) Rectangular CFST

Fig. 15. Effects of D/t (or D'/t) ratio on concrete stiffness of CFST columns.

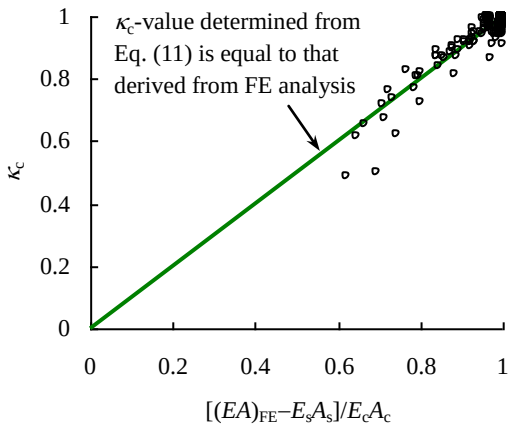

Fig. 16. Prediction accuracy of κ_c for circular CFST columns.

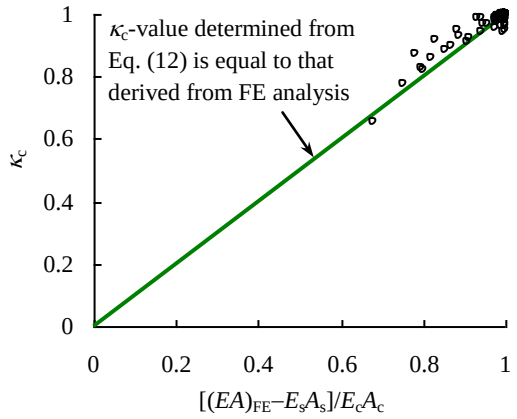

Fig. 17. Prediction accuracy of κ_c for rectangular CFST columns.

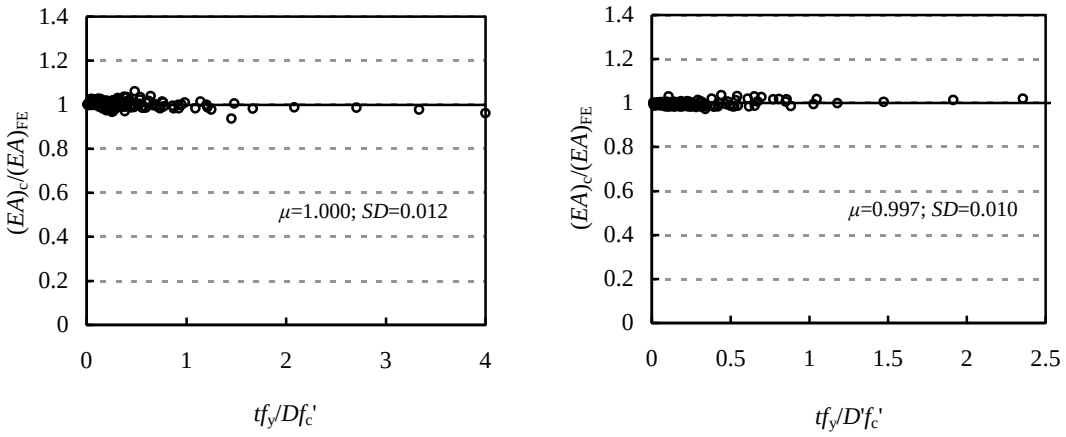

(a) Circular CFST (b) Rectangular CFST

Fig. 18. Comparison between $(EA)_c$ and $(EA)_{FE}$ of CFST columns.

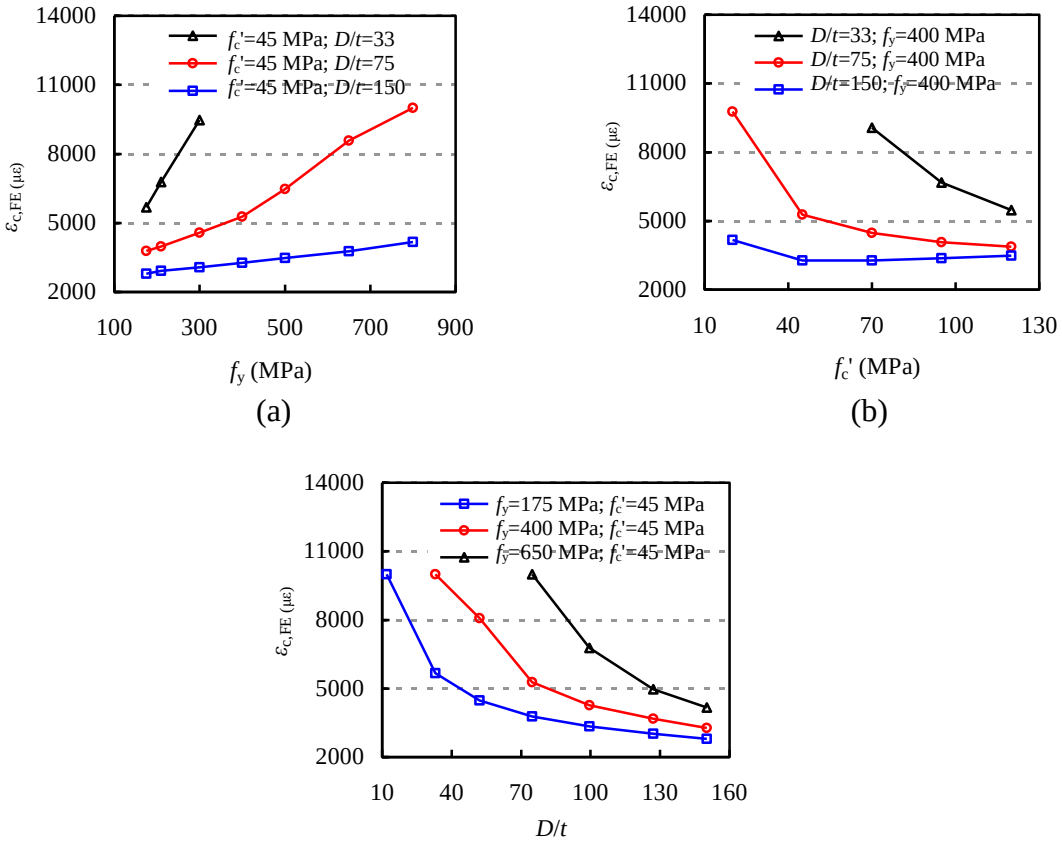

Fig. 19. Effects of f_y, f_c' and D/t ratio on compressive strains of circular CFST columns.

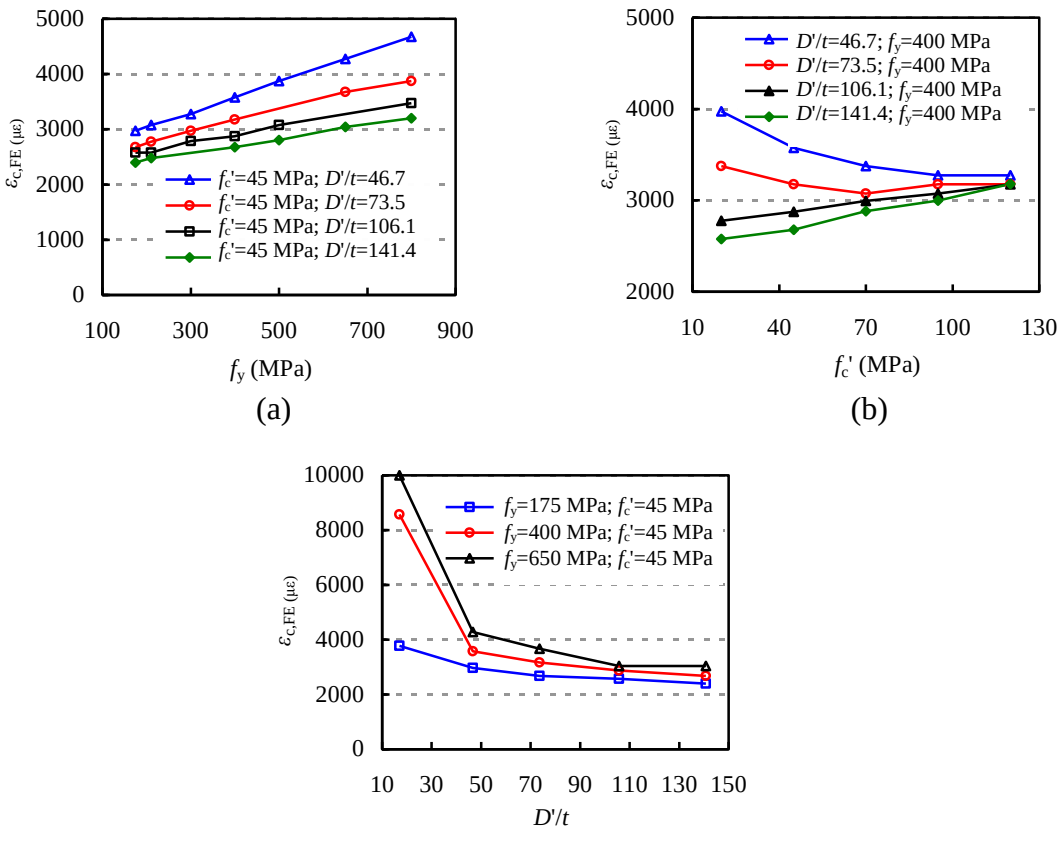

Fig. 20. Effects of f_y, f_c' and D'/t ratio on compressive strains of rectangular CFST columns.

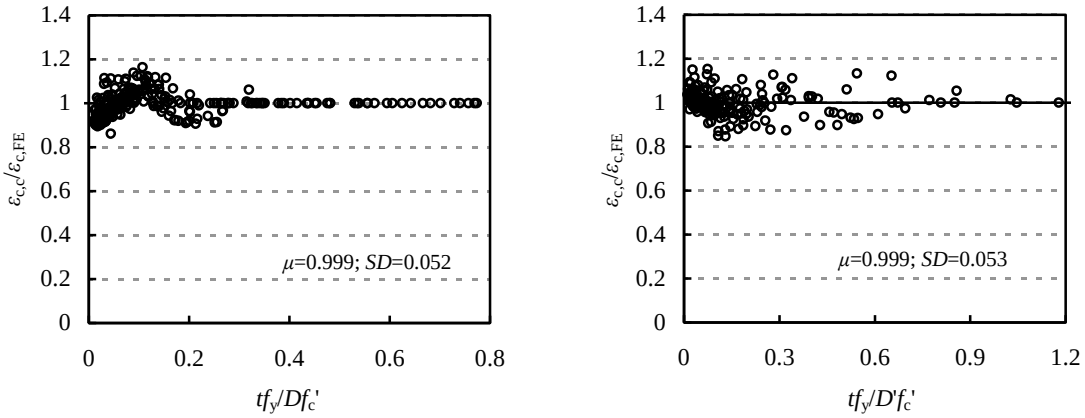

(a) Circular CFST (b) Rectangular CFST

Fig. 21. Comparison between $\varepsilon_{c,c}$ and $\varepsilon_{c,FE}$ of CFST columns.

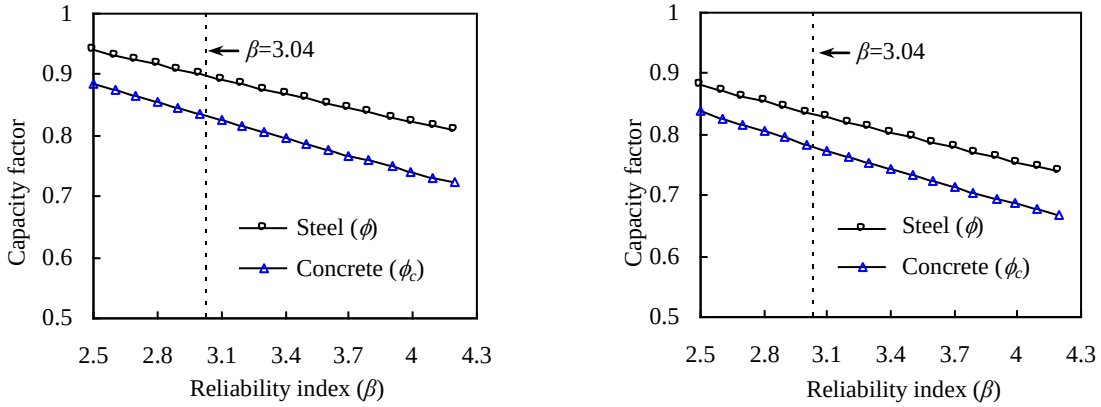

(a) Circular CFST (b) Rectangular CFST

Fig. 22. Capacity factor versus reliability index for CFST columns.

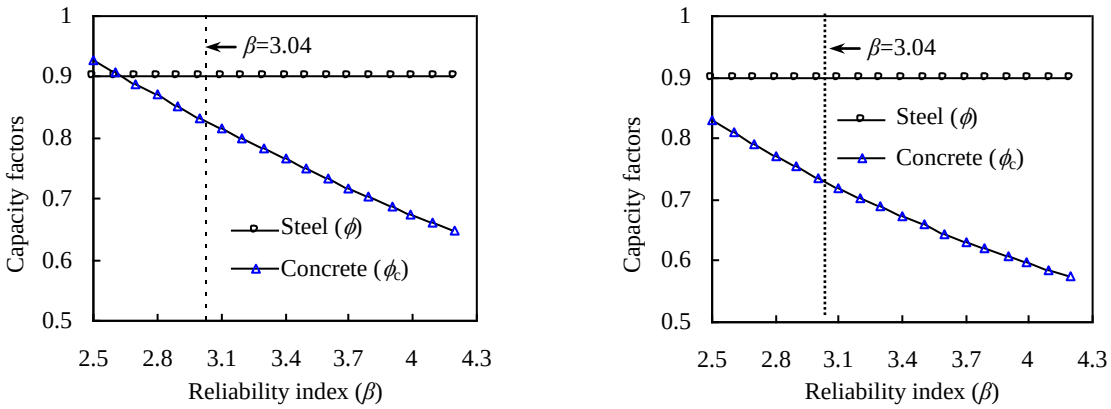

(a) Circular CFST (b) Rectangular CFST

Fig. 23. Concrete capacity factor versus reliability index when ϕ is taken as 0.9.

Table 1 Strength prediction methods and related limitations.

	Sectional type	Prediction of strength	D/t or H/t	f_y (MPa)	f_c' (MPa)
ACI	Circular	$N_u = A_s \cdot f_y + 0.85 f_c' \cdot A_c$	$D/t \le \sqrt{8E_s/f_y}$	–	$f_c' \ge 17.2$ MPa
	Rectangular		$H/t \le \sqrt{3E_s/f_y}$	–	$f_c' \ge 17.2$ MPa
AISC	Circular	$N_u = \begin{cases} [0.658^{(N_0/N_{cr})}]N_0 & (N_0 \le 2.25N_{cr}) \\ 0.877N_{cr} & (N_0 > 2.25N_{cr}) \end{cases}$ $N_0 = A_s \cdot f_y + 0.85 f_c' \cdot A_c$ $N_{cr} = \frac{\pi^2}{(KL)^2}(EI_{eff})$	$D/t \le 0.15E_s/f_y$	$f_y \le 525$ MPa	$21 \le f_c' \le 70$ MPa
	Rectangular		$H/t \le 2.26\sqrt{E_s/f_y}$	$f_y \le 525$ MPa	$21 \le f_c' \le 70$ MPa
AS 5100	Circular	$N_u = \eta_a f_y A_s + A_c f_c' \left(1 + \eta_c \frac{tf_y}{Df_c'}\right)$ $\eta_a = 0.25(3 + 2\bar{\lambda}) \le 1$ $\eta_c = 4.9 - 18.5\bar{\lambda} + 17\bar{\lambda}^2 \ge 0$	$D/t \le 82 \times 250/f_y$	$230 \le f_y \le 400$ MPa	$25 \le f_c' \le 65$ MPa
	Rectangular	$N_u = f_y A_s + A_c f_c'$	$H/t \le 35\sqrt{250/f_y}$	$230 \le f_y \le 400$ MPa	$25 \le f_c' \le 65$ MPa
EN1994	Circular	$N_u = \eta_a f_y A_s + A_c f_c' \left(1 + \eta_c \frac{tf_y}{Df_c'}\right)$	$D/t \le 90 \times 235/f_y$	$235 \le f_y \le 460$ MPa	$20 \le f_c' \le 60$ MPa
	Rectangular	$N_u = f_y A_s + A_c f_c'$	$H/t \le 52\sqrt{235/f_y}$	$235 \le f_y \le 460$MPa	$20 \le f_c' \le 60$ MPa
DBJ 13-51-2010	Circular	$N_u = f_{sc}(A_s + A_c)$; $\xi = \frac{A_s f_y}{A_c f_{ck}}$ $f_{sc} = (1.14 + 1.02\xi) \cdot f_{ck}$ for circular $f_{sc} = (1.18 + 0.85\xi) \cdot f_{ck}$ for rectangular	$D/t \le 150 \times 235/f_y$	$235 \le f_y \le 420$ MPa	$24 \le f_c' \le 70$ MPa
	Rectangular		$H/t \le 60\sqrt{235/f_y}$	$235 \le f_y \le 420$ MPa	$24 \le f_c' \le 70$ MPa

Table 2 Strength comparison between FE and simple calculations for circular CFST columns.

	Number of specimens	Eurocode 4 ($N_{EN}/N_{u,FE}$)				Current design method ($N_{uc}/N_{u,FE}$)			
		μ	SD	Maximum	Minimum	μ	SD	Maximum	Minimum
$tf_y/Df_c' < 0.5$	234	1.025	0.029	1.126	0.981	1.004	0.012	1.055	0.969
$tf_y/Df_c' \ge 0.5$	36	1.136	0.040	1.212	1.061	0.998	0.009	1.009	0.979

Table 3 Strength comparison between FE and simple calculations for rectangular CFST columns.

		Number of specimens	Eurocode 4 ($N_{EN}/N_{u,FE}$)				Current design method ($N_{uc}/N_{u,FE}$)			
			μ	SD	Maximum	Minimum	μ	SD	Maximum	Minimum
$tf_y/D'f_c' < 0.707$	$\frac{H}{t} > 100\sqrt{\frac{235}{f_y}}$	58	1.082	0.052	1.260	1.022	1.003	0.019	1.047	0.944
	$\frac{H}{t} \le 100\sqrt{\frac{235}{f_y}}$	155	0.986	0.030	1.040	0.878	0.989	0.012	1.022	0.958
$tf_y/D'f_c' \ge 0.707$		16	0.922	0.031	0.969	0.887	0.997	0.018	1.027	0.972

Table 4 COV of input parameters.

Variable	COV	References
Yield stress of steel (f_y)	0.07	[38]
Compressive strength of concrete (f_c')	0.10	[39], [40]
All linear dimensions (D, B, and H)	0.01	[6], [41]
Tube thickness (t)	0.10	[41]

Table 5 Reliability indices when the target reliability index is taken as 3.04.

Section type	Number of specimens	Capacity factors	
Circular	118	When ϕ is not fixed	$\phi = 0.90$ and $\phi_c = 0.83$
		When ϕ is fixed as 0.90	$\phi = 0.90$ and $\phi_c = 0.83$
Rectangular	177	When ϕ is not fixed	$\phi = 0.83$ and $\phi_c = 0.78$
		When ϕ is fixed as 0.90	$\phi = 0.90$ and $\phi_c = 0.74$